Sea-ice conditions in the Adélie Depression, Antarctica, during besetment of the icebreaker RV *Xuelong*

Mengxi ZHAI,[1]* Xinqing LI,[2,1]* Fengming HUI,[1] Xiao CHENG,[1] Petra HEIL,[3] Tiancheng ZHAO,[1] Tianyu JIANG,[1] Cheng CHENG,[1] Tianyu CI,[1] Yan LIU,[1] Zhaohui CHI,[4] Jian LIU[5]

[1]*State Key Laboratory of Remote Sensing Science, College of Global Change and Earth System Science, Beijing Normal University, Beijing, China*
E-mail: huifm@bnu.edu.cn, xcheng@bnu.edu.cn
[2]*College of Geomatics, Shandong University of Science and Technology, Qingdao, China*
[3]*Australian Antarctic Division and Antarctic Climate and Ecosystems Cooperative Research Centre, University of Tasmania, Hobart, Tasmania, Australia*
[4]*Department of Geography, Texas A&M University, College Station, TX, USA*
[5]*Polar Research Institute of China, Shanghai, China*

ABSTRACT. During the 30th Chinese Antarctic Expedition in 2013/14, the Chinese icebreaker RV *Xuelong* answered a rescue call from the Russian RV *Akademik Shokalskiy*. While assisting the repatriation of personnel from the Russian vessel to the Australian RV *Aurora Australis*, RV *Xuelong* itself became entrapped within the compacted ice in the Adélie Depression region. Analysis of MODIS and SAR imagery provides a detailed description of the regional sea-ice conditions which led to the 6 day long besetment of RV *Xuelong*. The remotely sensed imagery revealed four stages of sea-ice characteristics during the entrapment: the gathering, compaction, dispersion and calving stages. Four factors characterizing the local sea-ice conditions during late December 2013 and early January 2014 were identified: surface component of the coastal current; near-surface wind; ocean tides; and surface air temperature. This study demonstrates that shipping activity in ice-invested waters should be underpinned by general knowledge of the ice situation. In addition, during such activity high spatio-temporal resolution remotely sensed data should be acquired regularly to monitor local and regional sea-ice changes with a view to avoiding the besetment of vessels.

KEYWORDS: remote sensing, sea-ice dynamics

INTRODUCTION

Polar sea ice is an important part of the global climate system (Weller, 1993). Seasonal and interannual variations of sea-ice properties are wide-reaching, while local-scale variations, especially in coastal sea ice, can be transient, as they may be associated with short-term atmospheric or hydrological changes (Comiso, 2010; Mathiot and others, 2012). Such local sea-ice changes are likely to have a profound effect on ice characteristics, especially under convergence, with consequences not only locally but also in downstream regions. Furthermore, under conditions of global warming, the Antarctic sea-ice extent is increasing rather than decreasing (Parkinson and Cavalieri, 2012). Together these factors provide new challenges for Antarctic scientific expeditions, as well as for the resupply and staff turnover of Antarctic research stations. In the following we review the ice conditions surrounding the entrapment of two research vessels in the Mertz Glacier Polynya (MGP) region during austral summer 2013/14.

On 24 December 2013, the Russian RV *Akademik Shokalskiy* became entrapped in pack ice over the Adélie Depression (67°10′ S, 144°30′ E) following strong onshore winds. Unable to extract itself, the vessel sent the international distress signal. In response to this, the Chinese RV *Xuelong* diverted towards the Russian vessel on 25 December, approaching it on 27 December 2013. On 2 January 2014, RV *Xuelong* tendered helicopter support to enable the transfer of 52 passengers from RV *Akademik Shokalskiy* to the Australian RV *Aurora Australis*, which without helicopters on board waited near the outer ice edge. Unfortunately, by the end of the rescue operation, RV *Xuelong* found itself entrapped within the pack ice. On 7 January 2014, RV *Xuelong* was finally able to free itself from the pack ice, directed by scientific routing advice, which is presented here, derived from the analysis of remotely sensed imagery.

The two vessels were beset in the Adélie Depression region (Fig. 1), and to the northwest of Mertz Glacier Tongue (MGT). Along the coast, there are three bays: Commonwealth Bay, Watt Bay and Buchanan Bay. Iceberg B09B grounded in Commonwealth Bay in 2011 after calving of MGT in 2010. In late 2013 in the Adélie Depression, large areas of sea ice with a high sea-ice concentration of almost 100% existed, making water leads and ponds difficult to observe. In addition, a lot of slush ice was present in the Mertz Glacier Polynya area.

Based on remote-sensing images as well as ocean current, tidal and meteorological data, we analyzed sea-ice variability in the Adélie Depression from when RV *Xuelong* entered the pack ice. This was the first time a Chinese vessel had entered this area, and the consequent lack of weather and sea-ice information may have contributed to RV *Xuelong*

*These authors contributed equally to the work.

https://doi.org/10.3189/2015AoG69A007 Published online by Cambridge University Press

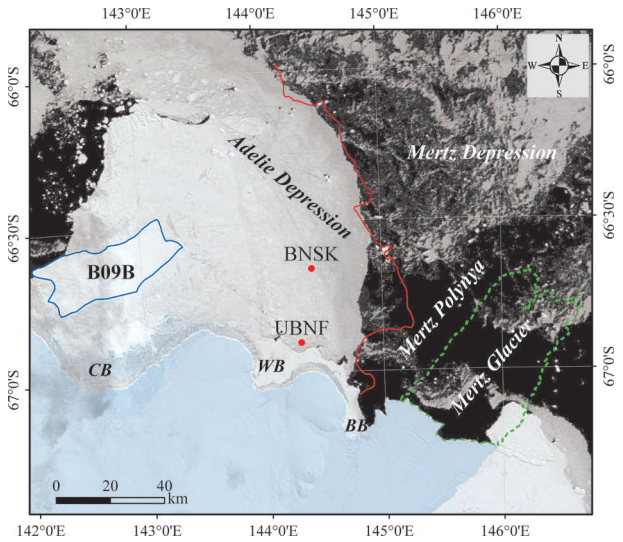

Fig. 1. Overview of the region of interest based on a MODIS image from 2 January 2014, showing the positions of both entrapped vessels (red dots; vessel call signs are annotated). UBNF and BNSK represent RV *Akademik Shokalskiy* and RV *Xuelong*, respectively. The primary topographic features include the Adélie Depression (AD), Commonwealth Bay (CB), Watt Bay (WB), Buchanan Bay (BB) and the Mertz Depression (MD). Also shown are the ice edge as of 29 December 2013 (red line) and the outline of Mertz Glacier Tongue (green dotted line) prior to its calving.

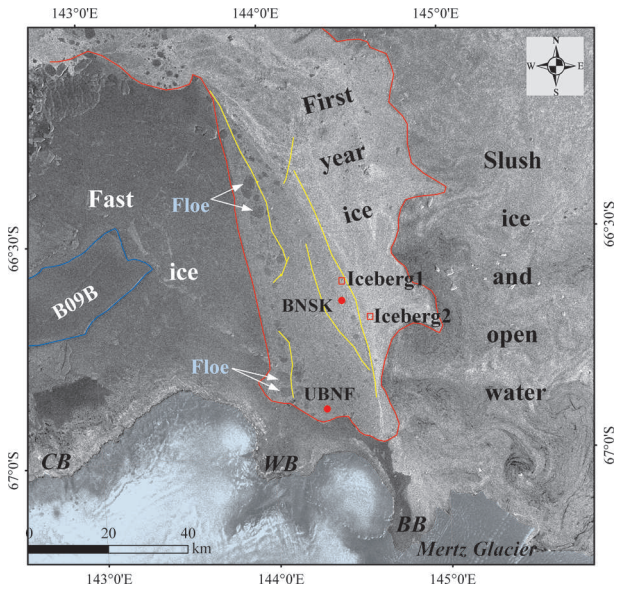

Fig. 2. RADARSAT-2 SAR image on 6 January 2014 providing details of the ice conditions in the region of interest, including first-year ice (polygon within red line), and active shearing (yellow lines). Red dots show position of vessels, as in Fig. 1. RADARSAT-2 Data and Products © MacDonald, Dettwiler and Associates Ltd (2014) – All Rights Reserved, and RADARSAT is an official mark of the Canadian Space Agency.

becoming entrapped. A detailed analysis of the ice conditions surrounding this incident may help to understand the processes of this area, and may also provide a reference for navigation in other ice-invested regions.

DATA

Three different types of data are used in this paper: remote-sensing data, meteorological data and tidal predictions. The remote-sensing data include Moderate Resolution Imaging Spectroradiometer (MODIS) and RARDARSAT-2 Synthetic Aperture Radar (SAR) images (Table 1). The meteorological and tidal prediction data are used to analyze causalities of the sea-ice variability. The meteorological data were acquired by the automatic weather station (AWS) on board RV *Xuelong*, and included wind direction, wind speed and air temperature. No tidal observation station exists in this area, so the tidal prediction data for Commonwealth Bay from the Australian Bureau of Meteorology are used.

RESULTS

General sea-ice condition

The region of interest was characterized by fast ice, first-year ice, icebergs, shear zones and slush ice (Fig. 2) based on the interpretation of the different backscattering coefficients (Jackson and Apel, 2004; Zakhvatkina and others, 2013). A large area of fast ice (~4620 km^2; Fig. 2) was identified to the northeast of iceberg B09B. Eastward of the fast ice, first-year

Table 1. MODIS and RADARSAT-2 SAR imagery used to characterize the sea ice in the region of interest

	Pixel spacing (ground range × azimuth)* m	Acquisition time (UTC)	Polarization mode/satellite	Beam mode
RADARSAT-2 SAR	50 × 50	10:37, 29 Dec 2013†	HH	ScanSAR Wide
	6.25 × 6.25	17:52, 31 Dec 2013†	HH	Multi-Look Fine
	6.25 × 6.25	10:50, 1 Jan 2014†	HH	Multi-Look Fine
	50 × 50	18:03, 3 Jan 2014	HH	ScanSAR Wide
	50 × 50	18:16, 6 Jan 2014	HH	ScanSAR Wide
	6.25 × 6.25	17:48, 7 Jan 2014	HH+HV	Multi-Look Fine
MODIS	250	05:20, 20 Dec 2013	Aqua	
		23:55, 2 Jan 2014	Terra	
		05:35, 3 Jan 2014	Aqua	
		23:30, 6 Jan 2014	Terra	
		05:10, 7 Jan 2014	Aqua	

*The product levels of all SAR data were in the Georeferenced Fine Resolution (SGF) format.
†Data available as JPG images from the Polar View Antarctic Node; other SAR images were purchased by Polar Research Institute of China.

https://doi.org/10.3189/2015AoG69A007 Published online by Cambridge University Press

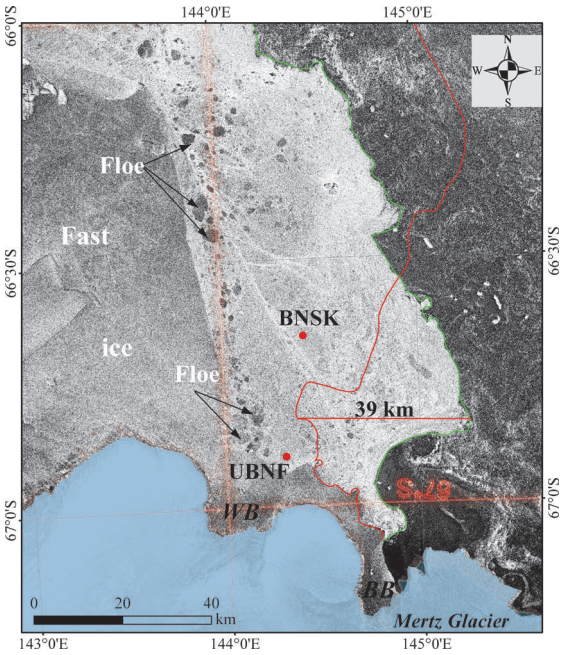

Fig. 3. Sea-ice edge changes during the gathering stage (RADARSAT-2, acquired on 29 December 2013). Also shown are the sea-ice edge on 20 December 2013 (red line) and 29 December 2013 (green line). Red dots show position of vessels, as in Fig. 1. RADARSAT-2 Data and Products © MacDonald, Dettwiler and Associates Ltd (2014) – All Rights Reserved, and RADARSAT is an official mark of the Canadian Space Agency.

ice was identified. Old and new ice were identified within the first-year ice, with the old ice located in the west and the new ice in the east. Vast floes of >2 km diameter were encountered in the western part of the first-year ice area near the fast ice, indicating broken-out fast ice from further east to the established first-year pack. We did not find any evidence of direct forcing of the fast ice on the evolution of the pack. On the other hand, a number of shear zones (yellow lines in Fig. 2), extending north-northwest, have been identified to the north of MGT. In our region of interest the general ice drift was to the north, with the first-year ice in the west moving slower than that further to the east. Shear zones were derived from the velocity gradient between the faster outer pack ice compared to the slower older sea ice, closer to the fast ice. Shear-induced ice deformation was the likely cause of linear patches of rough ice close to the shear zone.

Temporal sea-ice evolution

Over the relatively short interval from 20 December 2013 to 7 January 2014, the sea-ice condition changed dramatically. Four different stages of ice evolution were identified: gathering stage, compaction stage, dispersion stage and calving stage.

Gathering stage (20–29 December 2013)

Based on our analysis of RADARSAT-2 imagery, the ice-covered area within the region of interest increased >1000 km^2 over these 10 days. Associated with this, the sea-ice edge generally advanced seaward, especially along the southeastern corner of the region (Fig. 3), where it moved out by up to 39 km. Concurrent with this, the ice area of the northern section decreased into the previously ice-covered region. This differential response of the pack is consistent with the forcing of a cyclonic system, which had been observed a few days earlier. Associated with the advancing southern ice edge, the sea ice converged, increasing the ice concentration to nearly 100% with few open-water or thin-ice leads observed in situ (from the Russian vessel and RV *Xuelong*) or remotely (RADARSAT-2 imagery). Consequently, RV *Xuelong* became entrapped within the consolidating pack ice, which at this stage also included vast floes mainly in close proximity to the eastern edge of the fast ice. In fact, shear-induced ice deformation in pack ice was the driving reason for RV *Xuelong* to become entrapped. Both the presence of shear zones and their direct effect on sea-ice conditions prevented RV *Xuelong* from moving through the pack ice, which was under significant pressure. While RV *Xuelong* is an icebreaker ice-strengthened to class B1, designed to break ice as thick as 1.1 m (including 0.2 m thick snow) at 1.5 kn (2.8 km h^{-1}), under these conditions it could not move freely. Thus, encountering conditions exceeding her design specifications, RV *Xuelong* became beset.

Compaction stage (30 December 2013 to 2 January 2014)

This interval is marked by a significant decrease in sea-ice extent to the northwest of the continental shelf offshore of the Mertz Glacier region, by ~570 km^2 in the MODIS image acquired on 2 January 2014 (Fig. 1). In view of this loss in ice area, the pack remained under active compression, with new linear kinematic features visible in the MODIS image acquired on 2 January 2014 (Fig. 1). However, there were no open-water leads identified in the image, due to insufficient resolution in the MODIS image. At this stage, the wind blew consistently from the east, leading to sea-ice compaction and accumulation, resulting in sea-ice buckling and ridging. The surface temperature stayed low at ~–2°C, so little melt took place. At the same time, tidal predictions for Commonwealth Bay forecasted the monthly spring tides. This implies a rise in the sea level as the surface ocean water flocked towards the coast, the water pulling the sea ice with it towards the coast.

Dispersion stage (3–6 January 2014)

In comparing SAR images for 3 and 6 January 2014, we note that the sea-ice edge to the east of RV *Xuelong* advanced seaward (i.e. further eastward) by up to 6.6 km. However, the small-scale variability of the ice-edge displacement to the southeast of RV *Xuelong* was highly variable, exhibiting both ice-edge advance and sea-ice extent decrease. In addition, changes in backscatter intensity showed that the ice concentration of the enclosed pack decreased. The differential motion of two nearby icebergs to the southeast of RV *Xuelong* highlighted the active shear of the ice pack. From 3 to 6 January, iceberg 1 drifted ~10 km northwestward, coming within 8 km of RV *Xuelong* on 6 January. Iceberg 2 drifted in the same direction; its net translation was 8.2 km from 1 to 2 January, 8.5 km from 2 to 3 January and 2.7 km from 3 to 6 January (Fig. 4). The closest approach of iceberg 2 to RV *Xuelong* was to within 2.5 km on 2 January.

Calving stage (6–7 January 2014)

The major change during this stage was the break-up of first-year sea ice north of Watt Bay between 6 and 7 January 2014 (Fig. 5). Two linear kinematic features appeared near 144° E: the eastern line coincides with one of the shear

https://doi.org/10.3189/2015AoG69A007 Published online by Cambridge University Press

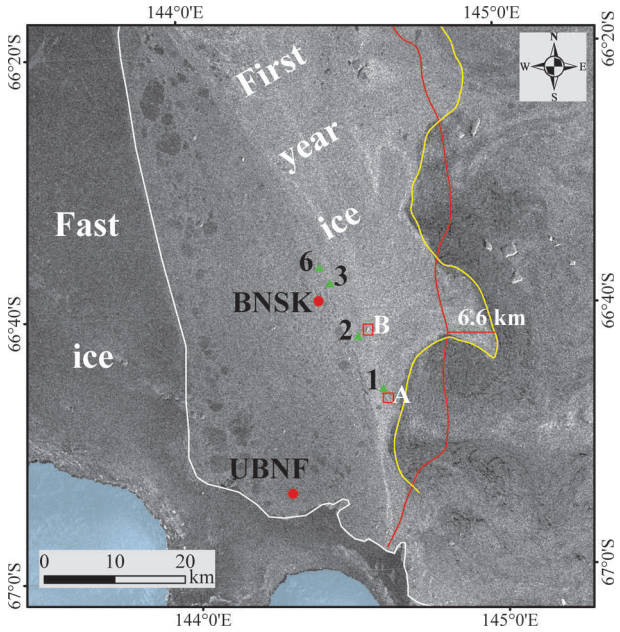

Fig. 4. RADARSAT-2 SAR image from 6 January 2014 showing the sea-ice edge for 3 January (red line) and 6 January (yellow line) as well as the border of the fast-ice area (white line). The red frames are the locations of iceberg 1 on 3 January and 6 January. The green triangles 1, 2, 3 and 6 are the locations of iceberg 2 on 1, 2, 3 and 6 January, respectively. Red dots show position of vessels, as in Fig. 1. RADARSAT-2 Data and Products © MacDonald, Dettwiler and Associates Ltd (2014) – All Rights Reserved, and RADARSAT is an official mark of the Canadian Space Agency.

zones depicted in Figure 2, namely the boundary of the old ice and the newer ice within the first-year zone. The western line resembles a further shear zone associated with the boundary of multi-year and first-year ice. On 7 January 2014, these two linear kinematic features widened, with the first-year ice separating from the fast ice. Open-water leads soon dominated the southern part of the old ice area adjacent to Watt Bay, enabling the pack there to break into several disparate sections. As the ice edge continued to advance, the occurrence of water ponds and leads increased as ice concentration declined rapidly.

At this stage the location of RV *Xuelong* was close to the boundary between new and old ice (Fig. 5), with the sea-ice concentration east of RV *Xuelong* decreasing further. Consequently RV *Xuelong* was advised to proceed south-eastwards, enabling her to break free of the ice.

DISCUSSION

Both RV *Xuelong*'s entrapment in and escape from the pack ice were closely related to the highly variable sea-ice conditions in the Adélie Depression. To explore this, we firstly review the regional setting. Before 2010, MGT blocked the westward advection of sea ice in the coastal current, giving rise to the Mertz Glacier Polynya on the western edge of MGT (Dragon and others, 2014). To the northeast of the Mertz Glacier Polynya, the blocking effect of numerous smaller grounded icebergs (also called the dagger) (Massom and others, 2001) and the large B09B iceberg gave rise to a second, albeit smaller polynya. Together these two formed a polynya system. New ice produced within this system was initially swiftly removed from the area by an offshore katabatic wind, resulting in a high net ice production rate. The salt precipitation associated with the formation of sea ice favors production of cold dense water. The cold dense water generated within this polynya system accounted for ~15–25% of the Antarctic Bottom Water (AABW) (Tamura and others, 2012; Dragon and others, 2014; N. Young, unpublished information). As AABW is the main driving force of the deep global ocean circulation with follow-on impact on the global climate system (Rintoul, 1998; Orsi and others, 1999), significant

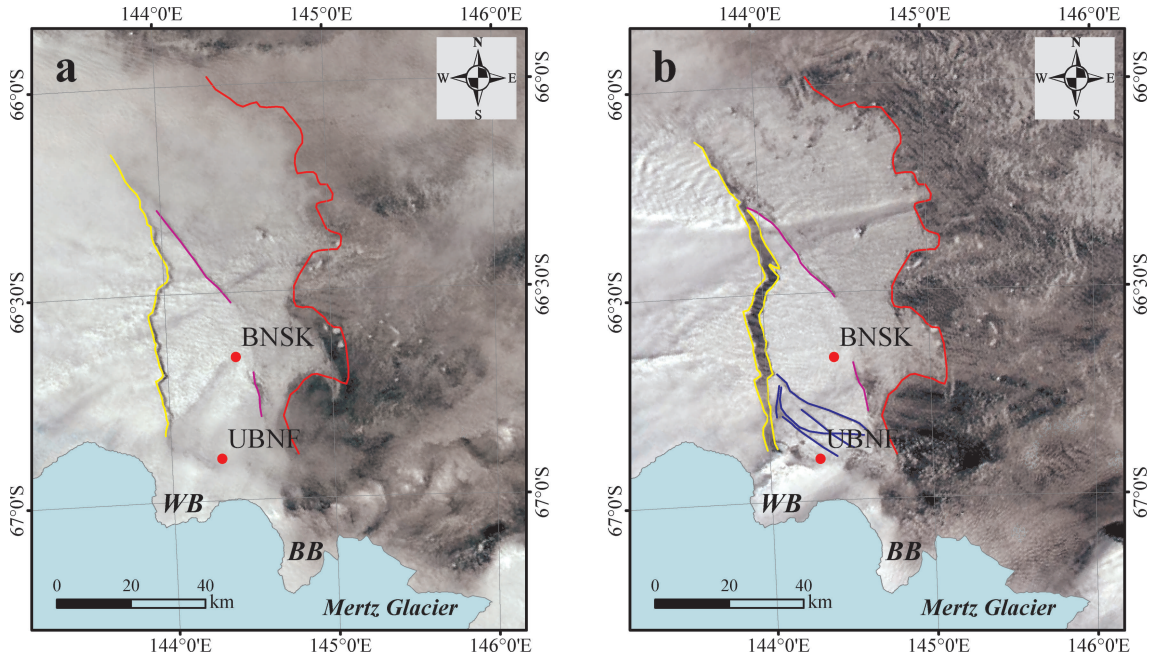

Fig. 5. Rapid changes in the ice edge and ice concentration, as seen from two consecutive MODIS images on (a) 6 January 2014 and (b) 7 January 2014. Also shown are the outer sea-ice edge (red lines), the zone delineating old from new sea ice (purple lines) and the zone delineating fast ice from first-year ice (yellow lines), and the open-water leads (blue lines). Red dots show position of vessels, as in Fig. 1.

https://doi.org/10.3189/2015AoG69A007 Published online by Cambridge University Press

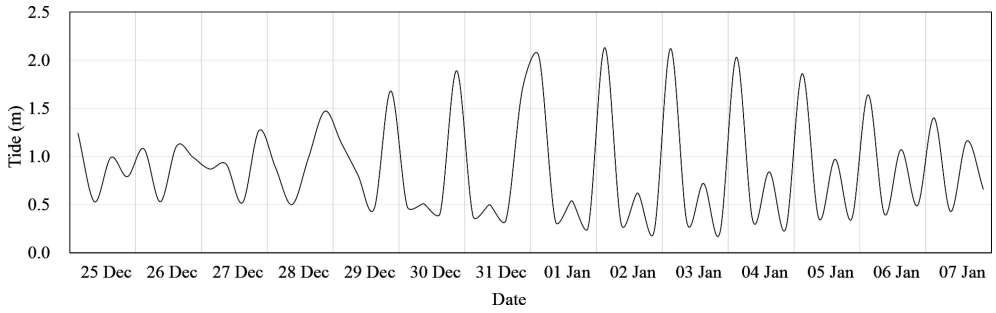

Fig. 6. Predictions of tidal elevation for Commonwealth Bay from 25 December 2013 to 7 January 2014.

changes within the Mertz Glacier Polynya system have global climatic consequences.

In February 2010, MGT calved after B09B collided with it; consequently becoming iceberg C28 (Legrésy and others, 2010; Young and others, 2010). While C28 drifted out of the area, B09B moved northwest across the Adélie Depression to ground in Commonwealth Bay in 2011. After the calving of C28, blocking decreased drastically, with analysis of remotely sensed data showing that the area of the Mertz Glacier Polynya reduced by ~70% (Dragon and others, 2014), while sea-ice production in the area reduced by 14–20% (Tamura and others, 2012). The MGT calving has a significant influence on both sea-ice production and distribution as well as on the polynya system of the Adélie and Mertz depressions.

The sea-ice variability is strongly associated with two processes: sea-ice drift and ice melt/freeze. The sea-ice drift is largely driven by the surface ocean currents and surface winds as well as by internal forcing, while the melt/freeze process is largely determined by thermodynamic processes.

Oceanic currents are a driving factor for sea-ice drift, especially in near-coastal regions (Worby and others, 1998; Heil and others, 2008). Concurrent with this, in the study area we identified two influences on the ocean current: the coastal and tidal currents. The former is associated with the East Wind Drift. Influenced by katabatic winds, this current is the counter-current to the Antarctic Circumpolar Current (Worby and others, 1998). The westward coastal current gives rise to accumulating ice behind topographic obstacles, and freezing converts it into fast ice, while in the lee of these obstacles thin ice or polynyas are encountered.

Tides are important as they modify the sea-ice drift through high-frequency (sub-daily) oscillations and are often associated with ice deformation (NSF, 1994). Predictions of tidal elevations for Commonwealth Bay show a spring tide on 2 January 2014 and a neap tide on 7 January 2014 (Fig. 6). In the region of interest, spring tides have a stronger influence moving sea ice towards the coast, and this reduces during the neap tide.

Atmospheric forcing due to wind-induced drag also modifies the sea-ice drift. From 25 December 2013 to 6 January 2014 (Fig. 7), the wind was persistently from the southeast, driving slush ice into the pack ice. Due to the presence of fast ice further west, this wind enlarged the pack-ice zone and consolidated the sea ice within the pack. At 18:00 UTC on 6 January 2014, the wind direction

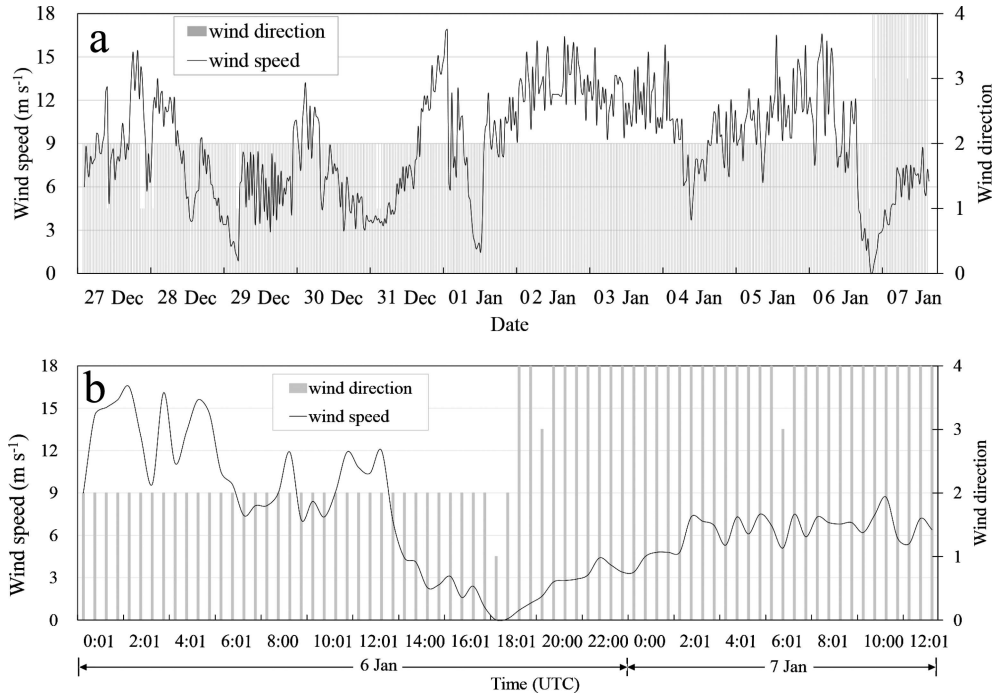

Fig. 7. Wind speed and direction from AWS aboard RV *Xuelong* measured at 35 m height (a) from 27 December 2013 to 7 January 2014 and (b) from 6 to 7 January 2014. Wind direction is shown in bins 1, 2, 3, 4 to represent 0–90°, 90–180°, 180–270° and 270–360°, respectively.

https://doi.org/10.3189/2015AoG69A007 Published online by Cambridge University Press

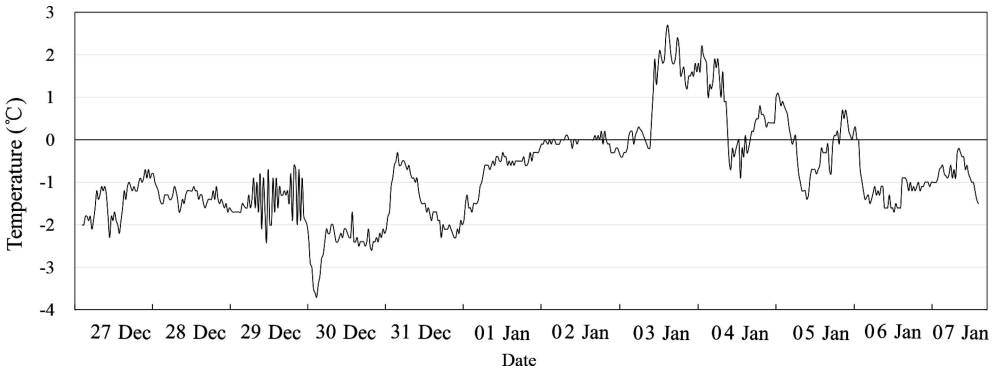

Fig. 8. Surface air temperature from AWS aboard RV *Xuelong* from 27 December 2013 to 7 January 2014.

changed to northwesterly, allowing the sea ice to spread into the open-water area. We note that higher-resolution measurements (or reporting) of wind direction would have been useful in predicting local change in ice conditions.

The hourly surface air temperature acquired by the AWS on board RV *Xuelong* shows low air temperature, around –2°C before 30 December 2013. Hence little melt occurred at this stage. At the beginning of the compaction stage (i.e. by late on 2 January 2014), the surface air temperature increased by ~2°C. During the third stage, the dispersion stage, the surface air temperature was higher, especially on 3 January, peaking just above 2.5°C (Fig. 8). Although there was some cooling immediately after this warm event, surface air temperature in the second half of this investigation generally remained above the freezing point of sea ice. Consequently, melt set in over the pack-ice area, initially removing the slushy ice, which had caused the compaction within the region. This sequence of factors led to sea-ice conditions that challenged the free progress of the two vessels.

CONCLUSIONS

The environmental conditions leading to the entrapment of RV *Xuelong* have been analyzed in near-real time with the aim of providing advice on possible exit options to the crew of the vessel. This relied on remotely sensed imagery to provide large-scale observations. Here we have used MODIS and SAR imagery to describe in detail sea-ice conditions in the Adélie Depression, where RV *Xuelong* was entrapped. The remotely sensed imagery clearly revealed sea-ice characteristics in four stages: the ice-gathering, compaction, dispersion and calving stages. Using in situ surface observations from RV *Xuelong*, together with tidal elevation predictions, the factors contributing to the sea-ice conditions encountered were assessed. We found that these forcing factors each played a contributory role during the four stages. Near-real-time access to the environmental data from the vessel would have been useful. Upgrades and standardization in the provision of underway meteorological and oceanographic data have been suggested, with a view to allowing ice condition analysis in support of future operational activities. The regular (hourly) conducting of underway observations following the Scientific Committee on Antarctic Research (SCAR) Antarctic Sea ice Processes and Climate (ASPeCt) protocol (Worby and Allison, 1999) has been recommended to assist the interpretation of near-real-time remotely sensed imagery.

ACKNOWLEDGEMENTS

This work was supported by the Chinese Arctic and Antarctic Administration, the National Natural Science Foundation of China (grant Nos. 41106157 and 41176163), the National Basic Research Program of China (grant No. 2012CB957704), the National High-tech R&D Program of China (grant Nos. 2008AA121702 and 2008AA09Z117) and the Fundamental Research Funds for the Central Universities. P.H. was supported by Australian Antarctic Science grant 4472 as well as by the Antarctic Climate and Ecosystems CRC program. We are grateful to RV *Xuelong* for providing weather data, to NASA for providing MODIS data, to the Polar View Antarctic Node website at the British Antarctic Survey for RADARSAT-2 SAR JPG images, and to the Australian Bureau of Meteorology for providing tidal predictions. We thank the anonymous reviewers for valuable comments.

REFERENCES

Comiso JC (2010) Variability and trends of the global sea ice cover. In Thomas DN and Dieckmann GS eds. *Sea ice*. Wiley-Blackwell, Oxford, 205–246

Dragon A-C, Houssais M-N, Herbaut C and Charrassin J-B (2014) A note on the intraseasonal variability in an Antarctic polynya: prior to and after the Mertz Glacier calving. *J. Mar. Syst.*, **130**, 46–55 (doi: 10.1016/j.jmarsys.2013.06.006)

Heil P and 6 others (2008) Tidal forcing on sea-ice drift and deformation in the western Weddell Sea in early austral summer, 2004. *Deep-Sea Res. II*, **55**(8–9), 943–962 (doi: 10.1016/j.dsr2.2007.12.026)

Jackson CR and Apel JR (2004) *Synthetic aperture radar: marine user's manual*. National Oceanic and Atmospheric Administration, US Department of Commerce, Silver Spring, MD http://www.sarusersmanual.com

Legrésy B, Lescarmontier L, Coleman R, Young N and Testut L (2010) Tidal rifting of the Mertz glacier tongue. *Geophys. Res. Abstr.*, **12**, EGU2010-9856

Massom RA, Hill KL, Lytle VI, Worby AP, Paget MJ and Allison I (2001) Effects of regional fast-ice and iceberg distributions on the behaviour of the Mertz Glacier polynya, East Antarctica. *Ann. Glaciol.*, **33**, 391–398 (doi: 10.3189/172756401781818518)

Mathiot P and 6 others (2012) Sensitivity of coastal polynyas and high-salinity shelf water production in the Ross Sea, Antarctica, to the atmospheric forcing. *Ocean Dyn.*, **62**(5), 701–723 (doi: 10.1007/s10236-012-0531-y)

National Science Foundation (1994) *Field manual for the United States Antarctic Program*. Office of Polar Programs, National Science Foundation, Washington, DC

Orsi AH, Johnson GC and Bullister JL (1999) Circulation, mixing, and production of Antarctic Bottom Water. *Progr. Oceanogr.*, **43**(1), 55–109 (doi: 10.1016/S0079-6611(99)00004-X)

https://doi.org/10.3189/2015AoG69A007 Published online by Cambridge University Press

Parkinson CL and Cavalieri DJ (2012) Antarctic sea ice variability and trends, 1979–2010. *Cryosphere*, **6**(4), 871–880 (doi: 10.5194/tc-6-871-2012)

Rintoul SR (1998) On the origin and influence of Adélie Land bottom water. In Jacobs SS and Weiss RF eds. *Ocean, ice and atmosphere: interactions at the Antarctic continental margin*. (Antarctic Research Series 75) American Geophysical Union, Washington, DC, 151–172

Tamura T, Williams GD, Fraser AD and Ohshima KI (2012) Potential regime shift in decreased sea ice production after the Mertz Glacier calving. *Nature Commun.*, **3**, 826 (doi: 10.1038/ncomms1820)

Weller G ed. (1993) *The role of the Antarctic in global change: an international plan for a regional research programme*. Scientific Committee on Antarctic Research, Cambridge

Worby AP and Allison I (1999) A technique for making ship-based observations of Antarctic sea ice thickness and characteristics, Part I: Observational technique and results. *Antarct. CRC Res. Rep.* 14

Worby AP, Massom RA, Allison I, Lytle VI and Heil P (1998) East Antarctic sea ice: a review of its structure, properties and drift. In Jeffries MO ed. *Antarctic sea ice: physical processes, interactions and variability*. (Antarctic Research Series 74) American Geophysical Union, Washington, DC, 41–67

Young N, Legrésy B, Coleman R and Massom R (2010) Mertz Glacier tongue unhinged by giant iceberg. *Austral. Antarct. Mag.* 18, 19

Zakhvatkina NY, Alexandrov VY, Johannessen OM, Sandven S and Frolov IY (2013) Classification of sea ice types in ENVISAT synthetic aperture radar images. *IEEE Trans. Geosci. Remote Sens.*, **51**(5), 2587–2600 (doi: 10.1109/TGRS.2012.2212445)

https://doi.org/10.3189/2015AoG69A007 Published online by Cambridge University Press